Applied Catalysis B: Environmental 322 (2023) 122107

Contents lists available at ScienceDirect

Applied Catalysis B: Environmental

journal homepage: www.elsevier.com/locate/apcatb

Low temperature catalytic conversion of CH_4, CO_2, and C_2H_4 to value-added C_3 oxygenates and olefins via C_1-C_2 coupling on Pd-Au/CeO_2

A.K.M. Kazi Aurnob [a], Kunlun Ding [a], Douglas R. Kauffman [b], James J. Spivey [a,*]

[a] Cain Department of Chemical Engineering, Louisiana State University, Baton Rouge, LA 70803, USA
[b] National Energy Technology Laboratory, US Department of Energy, Pittsburgh, PA 15236, USA

ARTICLE INFO

Keywords:
CH4 CO2
C-C coupling
Oxygenates
Low temperature
Pd-Au/CeO2

ABSTRACT

The catalytic conversion of CH_4 and CO_2 in the presence of more reactive co-reactants C_2H_4 and O_2 on Pd-Au/CeO_2 is achieved at 200 °C and elevated pressures. Propene and acetone were produced from the catalyzed reaction of CH_4 +C_2H_4 +O_2; addition of CO_2 to the reactant stream produced methyl acetate (MAc) but it significantly reduced the C-selectivities of propene and acetone. DRIFTS experiments confirmed the formation of methoxy species from CH_4 +CO_2 at 200 °C, which is an intermediate in the formation of MAc. Control experiments with blanks, and with CeO_2 did not show any propene, acetone, or MAc products. The complete oxidation of C_2H_4 was avoided; the catalyst is stable, and reactant conversions and product yields were sustained for the observed 1200 min time-on-stream, indicating that there is little or no carbon deposition and sintering. This direct coupling of CH_4 and C_2H_4 intermediates to higher carbon-number products at 200 °C is significant.

1. Introduction

Both methane (CH_4) and carbon dioxide (CO_2) are relatively abundant and inexpensive gases. CO_2 is a greenhouse gas and its conversion to other value-added chemicals along with that of CH_4 is extremely desirable due to the scientific challenges and commercial opportunities. However, CO_2 is kinetically stable because of the presence of strong C═O bonds, and it is inert in reaction with oxidants such as O_2 [1]. Nonetheless, when co-reacted with olefins, such as ethylene (C_2H_4), CO_2 can be activated without the need for extreme reaction conditions in the presence of a suitable catalyst [1]. The major component in natural gas is CH_4 and approximately 90 % of the produced natural gas is combusted globally for energy [2]. The combustion of CH_4 is preferred over its chemical conversion to value-added chemical because of the high kinetic stability of CH_4 [2,3]. Due to the kinetically inert nature of CH_4, extreme reaction conditions are required for chemical conversion. Typical CH_4 conversion processes include reforming to syngas, dehydroaromatization of methane for producing benzene, and oxidative coupling of methane (OCM) for producing C_2 hydrocarbons, all of which require high temperatures, typically 500–900 °C [4–6]. The direct coupling of CH_4 and CO_2 at relatively low temperatures is of paramount importance and a significant challenge for scientists.

The catalyst of choice in this work is Pd–Au/CeO_2. Pd can activate CH_4, CO_2, and C_2H_4 [3,7,8], it has been used in C-C coupling reactions to form acetic acid from CH_4 and CO_2 [9], and it is an established industrial catalyst for producing vinyl acetate from the coupling of acetic acid and ethylene [10–12]. Bulk Au is relatively inactive but Au nanoparticles (NP) can be highly active for various catalytic reactions [13], especially when supported on metal oxides [14]. Au has also been demonstrated to act as a promoter and improve the catalytic activity of Pd-based catalysts [15–17]. The addition of Au to Pd catalysts create more active, isolated Pd ensembles resulting from the synergistic effect of Pd and Au [8,10,18]. Gleich et al. suggested that Pd on Au matrix leads to an electronic modification of the active site in a Pd-Au system [19]. Both geometric and electronic effects are believed to be enhancing the activity of the active site when Au is added to Pd [19], but there are disagreements about which of the two effects is pronounced [8]. Although, the exact pathway by which Au increases the activity of Pd catalysts is unclear, there is general consensus that Pd-Au catalysts are more active than monometallic Pd catalysts in a number of reactions. Our objective is to catalytically activate CH_4, CO_2 and C_2H_4 and to facilitate catalytic C-C coupling to higher-carbon number products.

One major challenge of using an oxidizing environment is the undesired complete combustion of C_2H_4 to CO_2. Ceria (CeO_2) has redox properties, high oxygen storage capability and can act as an oxygen supplying buffer while alternatively removing excess oxygen from the

* Corresponding author.
E-mail address: jjspivey@lsu.edu (J.J. Spivey).

https://doi.org/10.1016/j.apcatb.2022.122107
Received 15 September 2022; Received in revised form 20 October 2022; Accepted 24 October 2022
Available online 28 October 2022

gas stream or reactant mixture [20,21]. The consumed O atoms from CeO_2 can be replenished from the O_2 reactant [20]. This indirect supply of oxygen from CeO_2 could inhibit the excessive over-oxidation of CH_4 and C_2H_4.

CeO_2 has been extensively studied for reactions involving CO_2. These include the methanation of CO_2, conversion of CO_2 to methanol, and nonreductive transformation of CO_2 [21]. Perhaps, a more relevant CeO_2-catalyzed reaction of CO_2 is the nonreduction transformation. In such a reaction, an H-containing reactant that can undergo dehydrogenation (such as R-OH and/or R-NH) is reacted with CO_2; examples of such reactions include the formation of carbonates (from CO_2 + R-OH), ureas (from CO_2 + R-NH) and carbamates (from CO_2 + R-OH + R-NH) [22]. Considering the redox and oxygen storage properties of CeO_2, it has been chosen as support for the Pd-Au catalyst studied here. We hypothesized that an oxygen-rich redox support, such as CeO_2, impregnated with Pd and Au could activate CH_4 and CO_2 and couple them with C_2H_4 in an oxygen-rich environment.

In this work, we synthesize and test a Pd-Au/CeO_2 catalyst to convert and couple CH_4 or CO_2 with C_2H_4 to form C_3 oxygenates and olefins. We present catalyst characterization data, such as BET surface area, TEM, DRIFTS, XRD, XPS, and XANES. We report the conversion of CH_4, CO_2, and C_2H_4, and the C-selectivities of the products of interest: propene, acetone, and MAc.

2. Experimental

2.1. Materials

Commercially available cerium (IV) oxide, CeO_2 (99.5 % REO), was purchased from Alfa Aesar (USA). Precursors $PdCl_2$ (99.999 % trace metal basis) and $HAuCl_4$•3 H_2O (99.9 % trace metal basis) were purchased from Acros Organics (USA) and Sigma-Aldrich (USA), respectively. Reactant gases and gas standards were purchased from Airgas (USA).

2.2. Catalyst preparation

Pd-Au/CeO_2 catalyst was prepared using deposition-precipitation method. The amounts of metal precursors used were determined so as to yield 1 wt% active metal in the final catalyst. Subsequently, appropriate amounts of $PdCl_2$ and $HAuCl_4$•3 H_2O precursors were taken in separate beakers and dissolved in deionized (DI) water to create two separate solutions. The two solutions were then mixed in a beaker with continuous stirring. CeO_2 dispersion was then added to the beaker while continuing stirring. The mixture was heated to about 40 °C and ammonium carbonate, $(NH_4)_2CO_3$, was added dropwise using a pipet to precipitate out the metals. Temperature was raised slowly to 75 °C and more $(NH_4)_2CO_3$ was added until the pH of the mixture was ~8. The mixture was then cooled to 30 °C and stirred overnight. Solids were separated from the mixture by vacuum filtration using a Büchner funnel followed by washing a few times with DI water. The obtained solid was then dried in an oven overnight at 105 °C. The dried catalyst was then calcined at 300 °C for 5 h followed by reduction in flowing H_2 at 250 °C for 4 h.

2.3. N_2 sorption

N_2 sorption experiments were carried out to determine the Breauner-Emmett-Teller (BET) surface area using an AMI-200 catalyst characterization system (Altamira Instruments Inc., USA) equipped with a TCD detector. Prior to N_2 sorption, the catalyst was kept at 120 °C for 4 h in flowing He to remove moisture. A three-point BET monolayer sorption was employed with N_2 concentrations of 10 %, 20 %, and 30 %, balance helium. The physio-chemical properties of the Pd-Au/CeO_2 catalyst are provided in Tables S1 and S2.

2.4. TEM

High Resolution Transmission Electron Microscopy (HR-TEM) was performed to observe the morphology of the surface. The d-spacings of the crystallite sites from the HR-TEM images were used to identify the species. HR-TEM was performed at LSU-SIF using a JEOL JEM-2011 Scanning TEM optimized for high resolution images at 200 kV.

High Angle Annul Dark Field (HAADF), Electron Diffraction Spectroscopy (EDS) and elemental mapping measurements were performed with double correctors Titan cubed Themis G2 operated at 300 kV from the Electron Microscopy Center (EMC) of Shared Equipment Authority (SEA) at Rice University. The microscope is equipped with Ceta camera, Gatan Quantum 966 energy filter and an electron monochromator.

2.5. DRIFTS

DRIFTS was carried out to identify the formation of surface species from the reactants and to verify the deposition of Pd and Au on CeO_2. DRIFTS was performed using a Thermo Scientific Nicolet 5700 FT-IR unit equipped with a mercury-cadmium-telluride (MCT) detector. A Harrick Praying Mantis™ DRIFTS attachment cell with KBr windows and sample holder was used. Samples were loaded in the DRIFTS cell and helium was flown at 100 sccm at 450 °C for an hour to remove moisture and impurities. The temperature was brought down to the reaction temperature of 200 °C and background spectrum was recorded with 64 scans and a spectral resolution of 4 cm^{-1} between the range 4000–650 cm^{-1}. Samples were then saturated with research grade CH_4 and CO_2 for a total of 30 min, during which adsorption spectra were recorded every 2 min with 16 scans at the same resolution and range as mentioned prior. The cell was then purged with helium to remove physisorbed and gaseous species; during this period, desorption spectra were recorded with the same equipment configuration and temporal frequency. To better understand the CH_4 +CO_2 reaction and the formation of bound species in the DRIFTS cell, CH_3OH vapor was adsorbed on fresh catalyst and then the two spectra were compared.

For DRIFTS experiments involving CH_3OH, fresh sample was pretreated in helium at 450 °C and background spectrum was taken at 200 °C using the aforementioned method. The sample was then placed in an open vial and the vial was placed inside a sealed container overnight containing 99.9 % CH_3OH (Alfa Aesar, USA) for adsorption of CH_3OH vapors. Sample with adsorbed CH_3OH was then placed in the DRIFTS cell, purged with helium and temperature was raised to 200 °C. Desorption spectra were recorded every 2 min in flowing helium using 16 scans with a spectral resolution of 4 cm^{-1} between the range 4000–650 cm^{-1}.

For CO-IR probing experiments, fresh sample was loaded in the cell and pretreated in helium at 120 °C for 30 min. The temperature was lowered to 25 °C and background spectrum was recorded with 64 scans at a spectral resolution of 4 cm^{-1} between the range 4000–650 cm^{-1}. Research grade CO was flown into the cell at 100 sccm to saturate the sample while adsorption spectra were recorded every 2 min with 16 scans at a spectral resolution of 4 cm^{-1} in the range 4000–650 cm^{-1}. Subsequent desorption spectra were recorded in flowing helium using the same configuration and temporal frequency.

2.6. XRD

X-ray powder diffraction (XRD) was performed to observe the crystal phases present in the prepared fresh catalyst and any changes in the spent catalyst samples. XRD was performed at LSU-SIF using a PANalytical Empyrean multipurpose diffractometer operated at 45 kV and 40 mA. Analyses were performed using Cu K_α radiation ($K_{\alpha2}$/ $K_{\alpha1}$ ratio of 0.5 was used with λ_1 = 1.5406 Å, and λ_2 = 1.5444 Å) and data were collected from 5° to 90° with a step size of 0.026°. XRD data were processed using PANAnalytical X′Pert software.

2.7. XPS

X-ray photoelectron spectroscopy (XPS) is primarily a surface analysis technique and was performed to quantify the surface loading of Pd and Au on CeO_2. XPS was performed at LSU-SIF using a Scienta Omicron ESCA 2SR X-ray Photoelectron Spectroscope with monochromatic Al K_α radiation (1486.7 eV) at a source voltage and power of 15 kV and 350 W, respectively. XPS peaks for Pd 3d and Au 4f spectra were calibrated using adventitious carbon C 1s peak at 284.8 eV and fitted using CasaXPS.

2.8. XANES

X-ray absorption near edge spectroscopy (XANES) was performed to investigate the changes in the valence state of the active metals between fresh and spent catalysts after reaction. XANES was performed at J. Bennett Johnston, Sr., Center for Advanced Microstructures and Devices (CAMD) of Louisiana State University. The electron storage ring at CAMD operates at 1.1 GeV with a beam current of 100 mA. L_{III} edge measurements of Pd were made at the double-crystal monochromator (DCM) beamline of CAMD which uses Lemonnier-type InSb 111 monochromator and has a maximum photon energy of 11 keV with an energy resolution of 1 eV. L_{III} edge measurements of Au were made at the wavelength shifter (WS)-DCM beamline which uses water-cooled Si 111 monochromator and has a maximum photon energy of 35 keV with an energy resolution of 2 eV. All the samples were dispersed on silicon-free and sulfur-free Kapton™ tapes and placed in the chamber for analysis. DCM beamline is equipped with a one element Ketek silicon drift detector having an area of 150 cm^2, and WS-DCM beamline is equipped with seven element Ketek silicon drift detectors with a combined area of 560 cm^2.

Pd metal standard L_{III} edge measurement was performed in a sealed chamber at 30 Torr and was measured in transmission mode; the obtained standard measurement was used to calibrate the monochromator at 3173 eV using the Pd white line. Pd L_{III} edge measurements of the samples were performed in the same chamber at 30 Torr but in fluorescence mode due to the samples having low Pd concentration. Au foil standard L_{III} edge measurement was performed in air and was measured in transmission mode; the obtained standard measurement was used to calibrate the monochromator at 11919 eV using the Au white line. Au L_{III} edge measurements from the samples were performed in air and in fluorescence mode. For each sample edge measurement, multiple spectra were collected and averaged to obtain a better signal to noise ratio. XANES spectra were processed and normalized using ATHENA and Larch software [23,24].

2.9. Catalytic reaction and reactant conversion

Catalyzed reactions that were investigated are (i) CH_4+CO_2+C_2H_4+O_2, (ii) CH_4+C_2H_4+O_2, and (iii) C_2H_4+O_2. Reaction (iii) serves as control to exclude the products obtained in this reaction as this work is focused on the products resulting from the involvement of CH_4 and/or CO_2. Fresh Pd-Au/CeO_2 samples were loaded into an AMI 200R HP reactor system (Altamira Instruments Inc., USA) equipped with a glass lined stainless steel tubular reactor in a fixed bed configuration. The reactor temperature was raised to the desired temperature of 200 °C and desired pressures of 6, 12, or 18 barg, depending on the reaction configuration. Initially, helium was flown through the reactor and reactant gases were only introduced once the desired set points had been reached. The gas hourly space velocity (GHSV) was 7600 h^{-1} for all reactions. For reaction involving CO_2 as a co-reactant, CH_4 and CO_2 were introduced into the reactor at 0 min. For reactions without CO_2 as a co-reactant, only CH_4 was introduced into the reactor at 0 min. For all the reactions, C_2H_4 and O_2 were added at 240 min and 288 min, respectively. From 288 min onward, all the reactants were simultaneously present in the reactor for a total time-on-stream of 1200 min.

These reactions (i-iii) were also employed at aforementioned reaction conditions initially with an empty reactor bed (blank runs) and then with calcined CeO_2 (without Pd or Au) fixed bed. The blank and CeO_2-only experiments serve as control and distinguish the products that are only produced on the catalyst Pd-Au/CeO_2.

The gaseous products were quantified downstream using an on-line Shimadzu GC2014 (1 FID, 2 TCD detectors) equipped with 3 Shimadzu MS-5A columns, 2 Shimadzu HSQ columns and a Restek RT-Q-BOND (30 m × 0.53 mm × 20 μm) column; products were identified in conjunction with a Shimadzu QP2010 GCMS equipped with a high-performance quadruple mass filter.

Conversions were calculated using Eq. (1), where R is either CH_4 or CO_2 or C_2H_4.

$$\%R_{conversion} = \frac{molar\ \ flow\ \ R\ \ in - \ \ molar\ \ flow\ \ R\ \ out}{molar\ \ flow\ \ R\ \ in} \times 100\% \quad (1)$$

Carbon Selectivity was based on CH_4 and was calculated using Eq. (2), where P is the product.

$$\%C_{selectivity} = \frac{molar\ \ flow\ \ P\ \ out}{mole\ \ of\ \ CH_4\ \ reacted} \times 100\% \quad (2)$$

3. Results and discussion

3.1. Catalyst evaluation

During catalyzed reactions, several products were observed that include ethane, acetaldehyde, propene, acetone, butene, and MAc. Although in smaller amounts, acetaldehyde was observed during blank runs and during CeO_2-only runs and was thus produced from the oxidation of C_2H_4 due to the presence of O_2. For this reason, we exclude acetaldehyde from products of interest. Butene was not observed in the blank runs or in the CeO_2-only runs, but it was only observed in the Pd-Au/CeO_2 catalyzed reactions involving CH_4 and/or CO_2. However, butene could most likely be produced from the coupling of two C_2H_4 molecules without the need for CH_4 or CO_2. Therefore, our results do not include acetaldehyde and butene, as the focus of this work is on products that involve the coupling of CH_4 and its intermediates.

There are two possible pathways for the formation of ethane in our reactions: the coupling of two CH_3* species ($2CH_4 \rightarrow C_2H_6 + H_2$) or the reduction of C_2H_4 to C_2H_6 ($C_2H_4 + H_2 \rightarrow C_2H_6$). However, we do not believe that the latter is possible because of the oxidizing environment of our reactions, thus ethane is likely produced from CH_4 ($2CH_4 \rightarrow C_2H_6 + H_2$). This observation serves as additional evidence for CH_4 activation and coupling. However, since ethane is not a C_3 species resulting from C_1-C_2 coupling, it has been excluded from this paper.

All the remaining products were only observed during catalyzed reactions and in the presence of CH_4. MAc was only observed in the reaction of CH_4+CO_2+C_2H_4+O_2 at 200 °C and 12 barg, i.e., MAc was not observed when CO_2 was absent. A summary of all the relevant products observed in our catalyzed reactions is provided in Table 1.

3.1.1. $CH_4 + CO_2 + C_2H_4 + O_2$ reaction

Propene, acetone, and MAc were produced from the catalyzed

Table 1
Summary of relevant products observed for different reactions at specific reaction conditions.

Reaction	Products		
	200 °C and 6 barg	200 °C and 12 barg	200 °C and 18 barg
$CH_4 + CO_2 + C_2H_4 + O_2$	Propene and acetone	Propene, acetone, and MAc	Propene and acetone
$CH_4 + C_2H_4 + O_2$	N/A	Propene and acetone	N/A
$C_2H_4 + O_2$	N/A	Propene (trace)	N/A

reaction of CH_4+CO_2+C_2H_4+O_2. This reaction was carried out at 200 °C and at pressures of 6, 12, and 18 barg. Although varying amounts of propene and acetone were observed at all pressures, MAc was only observed at 12 barg, and only in the presence of CO_2 as a reactant. This indicates that CO_2 plays a role in the formation of MAc, probably as a soft oxidizing agent, suggested from DRIFTS results (Section 3.4). The conversion and C-selectivities of relevant C_3 products are shown in Fig. 1. The conversion of both CH_4 and CO_2 changed little with time, remaining consistent around 10 % with a brief jump around 620 min (Fig. 1a); the conversion of both CH_4 and CO_2, especially that of CO_2, is significant at 200 °C.

Propene and acetone C-selectivities peaked right after the introduction of C_2H_4 and O_2 into the reactor as seen in Fig. 1b. This is understandable since C_2H_4 is required for the formation of propene (Scheme 1), and the oxidation of C_2H_4 to CH_3CHO is required prior to the formation of acetone (Scheme 2) as postulated in our mechanisms. C-selectivity of propene stayed fairly constant at around 0.1 %. The C-selectivity of MAc increased while that of acetone decreased with time. One explanation for this observation is that both acetone and MAc must compete for the CH_3CO* intermediate that is required for their formations (Schemes 2 and 3, step c), suggesting that MAc's formation would likely decrease the formation of acetone.

For reactions at 6 barg, we did not observe sustained conversion of the reactants. At 18 barg pressure, there was no sustained conversion of CH_4; moreover, CO_2 was produced from this reaction as opposed to being consumed, which is shown in Fig. S1a. The best result with respect to reactant conversions was obtained at a pressure of 12 barg and 200 °C.

3.1.2. $CH_4 + C_2H_4 + O_2$ reaction

Propene and acetone were produced from CH_4+C_2H_4+O_2 at 200 °C and 12 barg. The conversion of CH_4 peaked initially at 48 min, followed by a sharp decrease from 48 to 240 min. CH_4 conversion increased briefly again after the introduction of C_2H_4 at 240 min, and then started to decrease gradually after the introduction of O_2 at 288 min (Fig. 2a). CH_4 conversion stayed relatively constant at around 12 % from 900 min onward (Fig. 2a). Conversion of C_2H_4 after its introduction was relatively constant at around 20 %. C-selectivities of propene and acetone reached a maximum value of around 3.1 % and 1.5 %, respectively (Fig. 2b), which is much higher than those in the reaction with CO_2 co-reactant (CH_4+CO_2+C_2H_4+O_2). It should be noted that the inclusion of CO_2 as a reactant significantly decreases the C-selectivities of propene and acetone.

3.1.3. $C_2H_4 + O_2$ reaction

C_2H_4+O_2 reaction produced trace amounts of propene but this reaction produced neither acetone nor MAc. Significantly more propene was produced when CH_4 is added as a co-reactant. This suggests that CH_4 must be playing a role in the formation of propene and acetone.

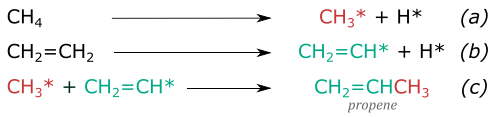

Scheme 1. Postulated mechanism for the formation of propene. Colors indicate the source of atoms.

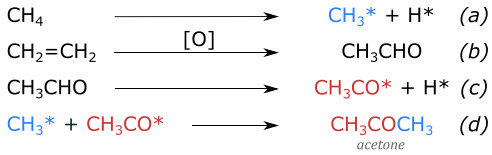

Scheme 2. Postulated mechanism for the formation of acetone. Colors indicate the source of atoms.

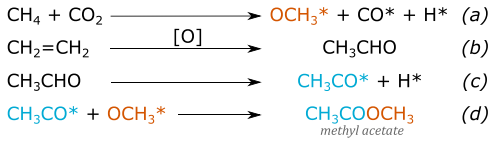

Scheme 3. Postulated mechanism for the formation of MAc. Colors indicate the source of atoms.

3.2. Evidence for CH_4 activation and coupling

The yields of propene and acetone are compared between reactions C_2H_4+O_2 and CH_4+C_2H_4+O_2; the only difference between them being the presence of CH_4 as a reactant. Yields of propene and acetone were calculated every 48 mins for a total of 1200 min for each reaction (C_2H_4+O_2 or CH_4+C_2H_4+O_2) and the distribution of product yields for each reaction are plotted as boxplots (Figs. S2 and S3). Insignificant quantities of propene and no acetone were observed as products from the catalytic reaction of C_2H_4+O_2. However, significantly greater quantities of propene and acetone were observed from catalyzed CH_4+C_2H_4+O_2 reactions.

Figs. S2 and S3 show the yield distribution of propene and acetone in mmol/hr, respectively. From the box plots, it is evident that the yield of both propene and acetone increases significantly when CH_4 is present as

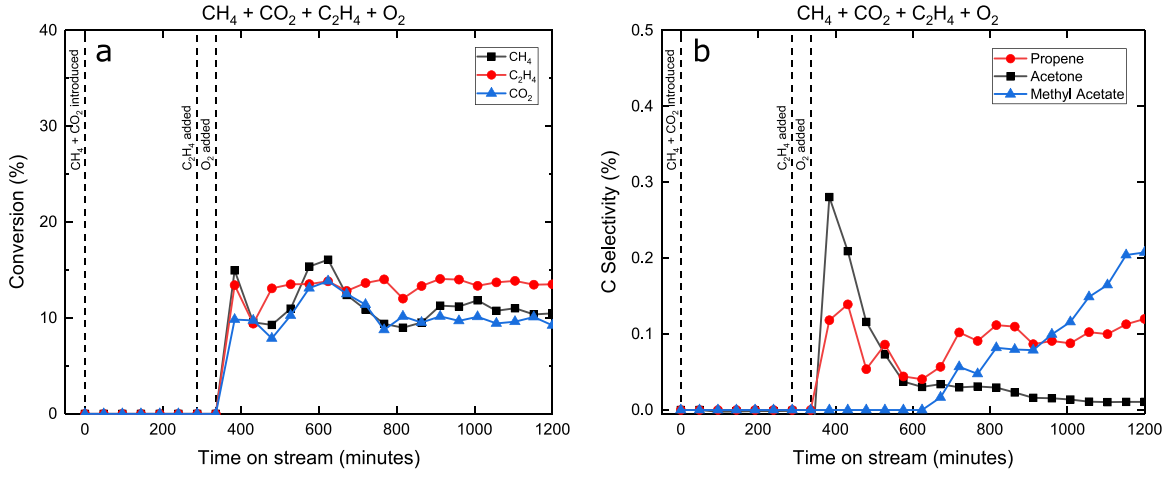

Fig. 1. Pd-Au/CeO_2 catalyzed CH_4 +CO_2 +C_2H_4 +O_2 reaction at 200 °C and 12 barg (a) conversion and (b) C-selectivities.

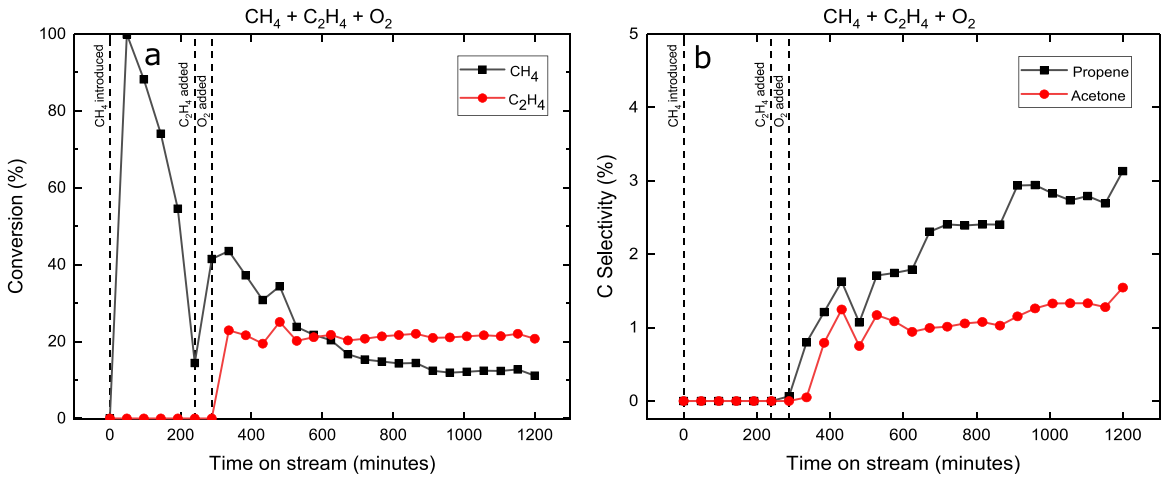

Fig. 2. Pd-Au/CeO_2 catalyzed CH_4 +C_2H_4 +O_2 reaction at 200 °C and 12 barg (a) conversion and (b) C-selectivities.

a reactant. A one-sided independent t-test was carried out to compare the yields of propene and of acetone in these two different reactions (C_2H_4+O_2 vs CH_4+C_2H_4+O_2). Both t-tests have a p-value ≈ 0, suggesting that the yields of propene and of acetone from these two reactions are statistically different and the addition of CH_4 as a co-reactant has significant impact in the yields of these C_3 products: propene and acetone. The only way addition of CH_4 as a reactant can produce more propene and acetone is by CH_4 reacting and coupling with C_2H_4 intermediates on the catalyst surface and forming the C_3 products.

3.3. XRD

XRD results for all the samples are shown in Fig. 3. The spectrum pattern for fresh Pd-Au/CeO_2 catalyst matches exactly with that of calcined CeO_2 and ICDD Card 00–004–0593 for CeO_2, indicating that Pd and Au are well dispersed and no large Pd or Au crystallite sites have formed. However, very small Pd and/or Au crystallite sites could be present that is not sensitive to XRD. The peaks observed for fresh Pd-Au/CeO_2 (Fig. 3c) are slightly broader than that of calcined ceria (Fig. 3b), suggesting there is a slight decrease in CeO_2 crystallinity due to the deposition of Pd and Au on CeO_2. No additional peaks are observed for the spent catalysts, indicating that no observable sintering has occurred, if any at all, since the reaction is carried out at a mild temperature of 200 °C.

3.4. DRIFTS

In our catalytic reactions, no gas phase products were observed from the reaction of CH_4+CO_2 alone. Hence, we used DRIFTS to investigate any surface intermediates that are forming from the reaction of CH_4+CO_2 and to better understand the role of CO_2 in the formation of MAc. CH_4 and CO_2 were co-fed over Pd-Au/CeO_2 catalyst at 200 °C and allowed to react for about 30 min. To eliminate peaks arising from gas phase CH_4 and CO_2 or physisorbed species, the cell was purged with helium and spectra were recorded while helium purging was in effect; this ensured that only the peaks arising from adsorbed surface species on the catalyst are recorded. The obtained results were compared to that of separate CH_4, CO_2, and CH_3OH DRIFTS experiments on Pd-Au/CeO_2.

The peaks at 2934 cm^{-1}, 2845 cm^{-1}, and 2722 cm^{-1} are for ν_a(CH) of methoxy, 2δ(CH) of methoxy, and 2δ(OCH) of formate species, respectively (Fig. 4a) [25–27]. These three peaks are observed only when both CH_4 and CO_2 are co-fed (CH_4-CO_2) and are verified by CH_3OH vapor adsorption spectrum over Pd-Au/CeO_2, but they are not seen when CH_4 and CO_2 are fed separately over Pd-Au/CeO_2. These peaks are also not seen when CH_4 and CO_2 are co-fed over calcined CeO_2, indicating that either one or more of the metal sites, particularly

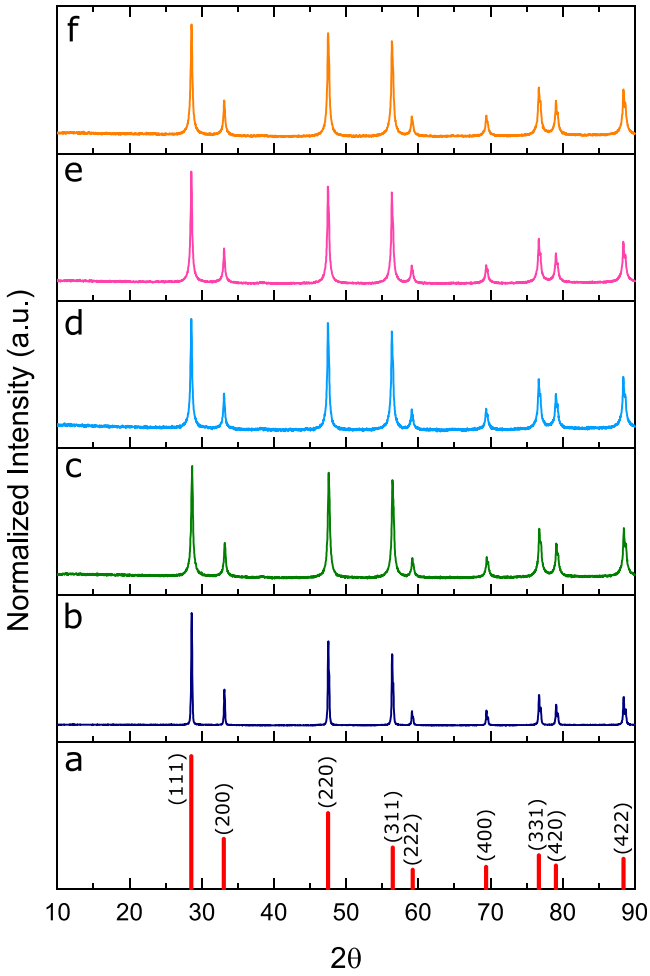

Fig. 3. XRD spectra for (a) ICDD Card 00–004–0593 for CeO_2, (b) calcined CeO_2, (c) fresh Pd-Au/CeO_2, (d) CH_4+CO_2+C_2H_4+O_2 spent, (e) CH_4+C_2H_4+O_2 spent, and (f) C_2H_4+O_2 spent.

Pd, PdO and Pd-Au bimetallics, on Pd-Au/CeO_2 are the active sites for CH_4 + CO_2 activation. Similar observations are also made at lower wavenumber region as shown in Fig. 4b. The peaks at 1548 cm^{-1}, 1371 cm^{-1}, and 1358 cm^{-1}, are caused by ν(CO) of formate, δ(OCH) of formate, and ν(CO) of formate species, respectively [26]. The peaks at 1548 cm−1 and 1358 cm^{-1} are only present for the CH_4-CO_2 and

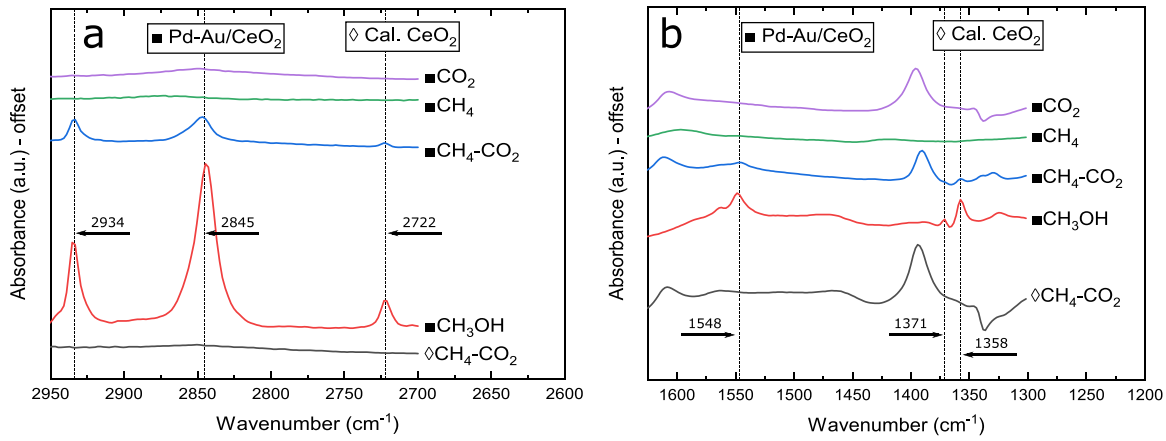

Fig. 4. DRIFTS spectra of CO_2 (lavender), CH_4 (green), CH_4-CO_2 (blue), CH_3OH (red) on Pd-Au/CeO_2, and CH_4-CO_2 on calcined CeO_2 (black) at (a) higher and (b) lower wavenumber regions.

CH_3OH spectra but not when CH_4 and CO_2 are fed separately over Pd-Au/CeO_2. The 1371 cm^{-1} peak is relatively stronger for CH_3OH spectrum compared to a weak shoulder for the CH_4-CO_2 spectrum, suggesting the δ(OCH) of formate is weaker for the CH_4-CO_2 spectrum.

Methoxy is believed to form from the partial oxidation of CH_4 to CH_3O* by CO_2. However, the formate species could be formed via two pathways: (1) due to the reduction of CO_2 to HCOO* or (2) due to further oxidation of methoxy species from CH_3O* to HCOO*, with CO_2 being the source of oxygen. If so, methoxy is formed in-situ, which then leads to the formation of MAc as postulated in the reaction mechanism (Scheme 3).

This demonstrates that CH_4 and CO_2 reacted on Pd-Au/CeO_2 at 200 °C to form methoxy and formate species, meaning this catalyst can activate both CH_4 and CO_2 at low temperature. CO_2 works as an oxidant to oxidize CH_4 to form methoxy species, as reported to do so at high temperatures [28], but we observe this reaction at low temperatures on Pd-Au/CeO_2.

3.5. XPS and XANES

Au 4f and Pd 3d photoelectron spectra for the fresh catalyst and for the spent samples are shown in Figs. 5a and 6, respectively. The peaks were fitted by implementing area constraints and position constraints obtained from literature due to the data being noisy, particularly for Pd 3d.

Characteristic Au $4f_{7/2}$ and Pd $3d_{5/2}$ are reported to be around 84.5 eV and 335.7 eV for Au/CeO_2 and Pd-Au, respectively [29,30]. Typically, the $4f_{7/2}$ peak is expected to shift to a higher binding energy (BE) for Au^{1+} species on CeO_2 (85.8 eV) [29]. However, a decrease in the BE for Au $4f_{7/2}$ to c.a. 83.5 eV is observed for all the samples as shown in Fig. 5a. This indicates that Au is present as Au^0 on the surface and Pd-Au bimetallics have been formed on the surface, causing this downward shift in BE for Au $4f_{7/2}$ [31–33]. This Pd-Au bimetallic formation is also confirmed by XANES (Fig. 5b) and TEM-EDS (Figs. S6 and S7). The BE and the oxidation state of Au does not change for the spent catalysts as observed from the XPS.

The Au L_{III} edge corresponds to the electron transition from $2p_{3/2}$ to

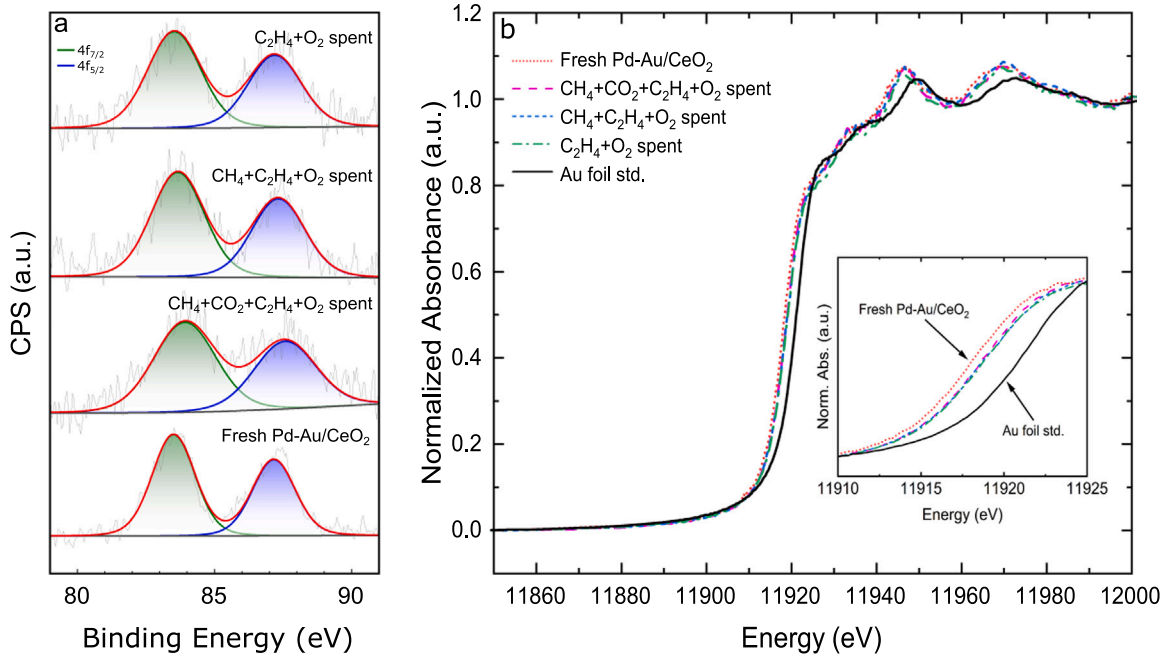

Fig. 5. (a) XPS curve fitting for Au 4f photoelectrons; the gray curve refers to the raw data and red curve is the overall fitted data, (b) Au L_{III} edge XANES (inset: zoomed in).

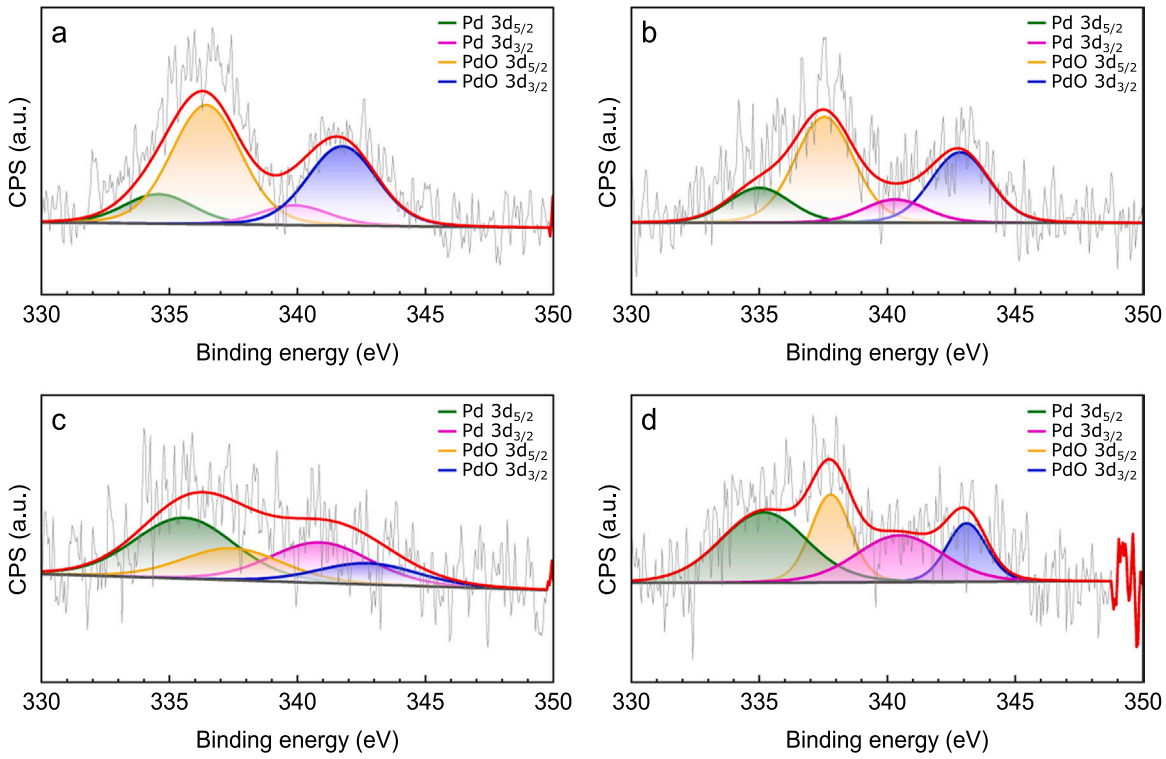

Fig. 6. XPS curve fitting for Pd 3d photoelectrons. They gray curve refers to the raw data and red curve is the overall fitted data for (a) fresh Pd-Au/CeO_2, (b) CH_4+CO_2+C_2H_4+O_2 spent, (c) CH_4+C_2H_4+O_2 spent, and (d) C_2H_4+O_2 spent samples.

5d or 6s orbitals [34]. The Au L_{III} spectra of all the Pd-Au/CeO_2 samples (fresh and spent) are similar in shape with small shifts in edge energy (E_0) between them. However, these spectra are significantly different in shape and E_0 to that of Au foil standard, suggesting interaction between Pd and Au in Pd-Au/CeO_2, and Pd-Au bimetallic has been formed in the catalyst (Fig. 5b) [32], which is consistent with TEM-EDS (Figs. S6 and S7). Fresh Pd-Au/CeO_2 has the lowest Au L_{III} edge energy whereas the spent catalyst from CH_4+C_2H_4+O_2 reaction has the highest edge energy with a difference in E_0 of about 0.7 eV between them (Fig. 5b). Increase in Au L_{III} E_0 could arise from the bond formation of Au with more electronegative ligands, such as O [34] or due to the isolation of Au from Pd-Au bimetallics in the bulk.

For Pd 3d XPS, it was clear that PdO is also present alongside Pd, and the peaks were fitted for both Pd and PdO [30,35]. Pd, Pd-Au, and PdO are all different forms of Pd present on the surface. The characteristic Pd $3d_{5/2}$ peak position for PdO species is at 338 eV, which is very close to the fitted PdO $3d_{5/2}$ peak positions ~337.5 eV [30]. The fresh catalyst (Fig. 6a) has the highest PdO:Pd ratio compared to all the spent catalysts; all the spent catalysts get reduced to some degree, forming more Pd (Fig. 6b-d) than that of the fresh sample, which is consistent with Pd L_{III} XANES shown in Fig. 7. For the spent catalyst from reaction CH_4+C_2H_4+O_2, data fitting revealed that there is relatively more of Pd than PdO on the surface (Fig. 6c), meaning this is the most reduced sample and this is also in agreement with Pd L_{III} XANES. This could be due to the presence of O_2 as the only oxidant (CO_2 is not used as a reactant in this reaction) and the uptake of oxygen is greater since both CH_4 and C_2H_4 are partially oxidized to form acetone. This relative scarcity of oxygen here likely aided the transformation of surface PdO→Pd (Fig. 6c).

The Pd L_{III} edge spectra for the fresh and spent catalyst samples are shown in Fig. 7. The white line intensity for Pd standard powder is very weak due to the lack of 4d holes in Pd metal [36]. However, for the catalyst samples, a strong white line is observed which is caused by electron transition from $2p_{3/2}$ to $5d_{3/2}$ and $5d_{5/2}$ [36]. The shift in E_0 and the increase in white line area intensity is directly proportional to the

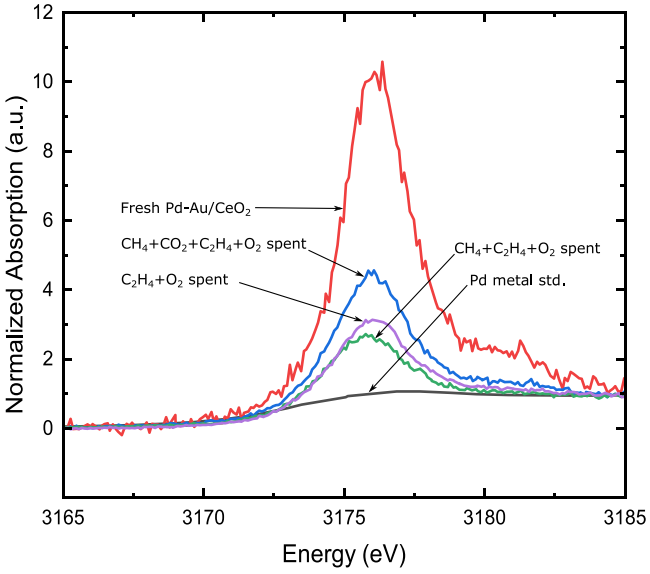

Fig. 7. Pd L_{III} edge spectra for Pd metal standard, spent Pd-Au/CeO_2 after CH_4+C_2H_4+O_2 reaction, spent Pd-Au/CeO_2 after C_2H_4+O_2 reaction, spent Pd-Au/CeO_2 after CH_4+CO_2+C_2H_4+O_2 reaction, and fresh Pd-Au/CeO_2.

oxidation number of Pd [36,37]. In our experiment, white line intensity and white line area intensity for the fresh catalyst is the highest and they decrease for the spent catalysts, suggesting that Pd is relatively more oxidized initially in the fresh catalyst and is reduced during the reaction in the spent samples. This is likely due to the catalyst acting as partial oxidant for the reactants and is reduced in the process. It is well established that the Pd exists as PdO on CeO_2 support and that PdO is generally thermally stable on CeO_2 at very high temperatures [38]. In this work, the reaction temperature is a mild 200 °C and it is not

expected that a PdO→Pd transformation is occurring due to thermal instability of PdO at this low temperature. Hence, a more likely explanation is that PdO is reduced by the reaction with the reactants and is transforming chemically to Pd.

3.6. Postulated reaction mechanisms

Reaction mechanisms for the formation of propene, acetone and MAc are shown in Schemes 1, 2, and 3, respectively. We have also proposed reaction networks in Figs. S13 and S14 for the two reactions, but future in-situ spectroscopic, kinetic, isotopic, and computational studies are required to validate our hypothesis and identify the precise reaction pathways, intermediates, and rate determining steps.

The dissociative adsorption of methane shown in both Schemes 1 and 2 steps (a) are widely reported in literature to occur over Pd-based and Pd/CeO_2 catalysts [39–43]. Similarly, (from Scheme 1 step (b)) the dissociative adsorption of C_2H_4 has been reported in literature to occur over Pd, Pd-based, and Pd-Au catalysts [16,44–46]. Based on DRIFTS results, we propose that CO_2 oxidizes CH_4 to CH_3O^* species (Scheme 3 step (a)); the formed CH_3O^* then takes part in the reaction to form MAc. The oxidation of C_2H_4 to acetaldehyde shown in Schemes 2 and 3 steps (b) has been reported in literature to take place over Pd, Pd-Au bimetallics, and other supported Pd catalysts [47–49]; the dehydrogenation of acetaldehyde shown in Schemes 2 and 3 steps (c) has also been reported in literature to take place over Pd/CeO_2 catalysts [50].

3.7. Discussion

Both CH_4 and CO_2 are kinetically stable gases and requires high temperature for chemical conversion. Relatively more explored chemical conversion processes of CH_4 include dry reforming and dehydroaromatization of methane to produce syngas (CO and H_2) and benzene, respectively [5,6,51]; both pathways require high temperatures (>500 °C). Oxidative Coupling of Methane (OCM) is another chemical conversion alternative, but this also requires very high temperatures (>800 °C) [6]. As a result, CH_4 is generally flared around the world to produce energy, contributing to CO_2 emissions. If the catalytic conversion of CH_4 to value-added chemicals with high C-selectivity at relatively mild conditions is achieved, it could become financially attractive to implement these conversion processes instead of flaring CH_4. Milder reaction conditions could entice commercialization of CH_4 and CO_2 conversion processes and reduce the release of these greenhouse gases into the atmosphere. The conversion of both CH_4 and CO_2 at mild conditions would be feasible when coupled with olefins (C_2H_4) to produce higher-value products.

To our best knowledge, the lowest temperature at which CH_4 bond cleavage was achieved was in the presence of O_2 on IrO_2 (110) surface at 150 K (−123.15 °C) producing CO_2, CO and H_2O [52]. Low-temperature dry reforming reaction between CH_4 and CO_2 was reported to occur at 400 °C achieving only 2% conversion on Zn promoted Ni/SiO_2 [53]. Xiao et al. achieved 10 % conversion of CH_4 on Pd/CeO_2 surface at 224 °C, in the combustion reaction of CH_4 [54]. In our work, we have demonstrated that both CH_4 and CO_2 have been activated at 200 °C, and CH_4 has coupled with C_2H_4 intermediates to form C_3 olefins and oxygenates on multi-functional $Pd\text{-}Au/CeO_2$.

4. Conclusion

In this work, we have demonstrated the conversion of CH_4 and CO_2 with co-reactants C_2H_4 and O_2, to C_3 products such as propene (C_3H_6), acetone (C_3H_6O), and methyl acetate ($C_3H_6O_2$). In addition to its commercial potential, the scientific interest in the catalytic coupling both CH_4 and/or CO_2 with olefins to form higher carbon-number products is significant. The multifunctional catalyst in this work, $Pd\text{-}Au/CeO_2$, has demonstrated the following at a mild temperature of 200 °C: (a) CH_4 activation, (b) CO_2 activation, (c) partial oxidation of reactants, and (d) C-C coupling to produce higher carbon products. Moreover, the catalyst is stable at 200 °C and the conversion of reactants were sustained for the observed 1200 min without any observable coke formation or sintering. We found that the optimum reaction pressure is 12 barg, beyond which most of the C_2H_4 is combusted to CO_2. This work demonstrates and serves as proof-of-concept that the conversion of CH_4 and CO_2 at low temperature is possible. Further study of the mechanism, long-term stability is underway.

Disclaimer

Portions of this report were prepared as an account of work sponsored by an agency of the United States Government. Neither the United States Government nor any agency thereof, nor any of their employees, makes any warranty, express or implied, or assumes any legal liability or responsibility for the accuracy, completeness, or usefulness of any information, apparatus, product, or process disclosed, or represents that its use would not infringe privately owned rights. Reference herein to any specific commercial product, process, or service by trade name, trademark, manufacturer, or otherwise does not necessarily constitute or imply its endorsement, recommendation, or favoring by the United States Government or any agency thereof. The views and opinions of authors expressed herein do not necessarily state or reflect those of the United States Government or any agency thereof.

CRediT authorship contribution statement

A. K. M. Kazi Aurnob: Conceptualization, Investigation, Formal analysis, Visualization, Writing – original draft. **Kunlun Ding:** Conceptualization, Writing – review & editing. **Douglas R. Kauffman:** Conceptualization, Writing – review & editing. **James J. Spivey:** Conceptualization, Resources, Supervision, Project administration, Funding acquisition, Writing – review & editing.

Declaration of Competing Interest

The authors declare that they have no known competing financial interests or personal relationships that could have appeared to influence the work reported in this paper.

Data availability

Data will be made available on request.

Acknowledgement

Authors would like to acknowledge the financial support for this work provided by University Coalition for Fossil Energy Research (UCFER) funded by the U.S. Department of Energy (DOE) under grant number 5956-LSU-DOE-6825/ DE-FE0026825 through National Energy Technology Laboratory (NETL) and Penn State University. Authors greatly appreciate the help of LSU CAMD's Dr. Amitava Roy for his help with Pd and Au L_{III} edge XANES experiments and Dr. Orhan Kizilkaya for his suggestions in XPS data processing. Authors are thankful to Dr. Dongmei Cao and Dr. Yang Mu of LSU SIF for their help with performing TEM, XRD, and XPS. Authors are also thankful to Rice University EMC and Dr. Guanhui Gao for her assistance in performing TEM at Rice University.

Appendix A. Supporting information

Supplementary data associated with this article can be found in the online version at doi:10.1016/j.apcatb.2022.122107.

References

[1] E. Alper, O. Yuksel, Orhan, CO2 utilization: developments in conversion processes. Petroleum 3 (1) (2017) 109–126.
[2] R. Horn, R. Schlögl, Methane activation by heterogeneous catalysis, Catal. Lett. 145 (1) (2014) 23–39.
[3] P. Tang, et al., Methane activation: the past and future, Energy Environ. Sci. 7 (8) (2014) 2580–2591.
[4] L. Sun, et al., Methane activation and utilization: current status and future challenges, Energy Technol. 8 (2019) 8.
[5] J.J. Spivey, G. Hutchings, Catalytic aromatization of methane, Chem. Soc. Rev. 43 (3) (2014) 792–803.
[6] V. Havran, M.P. Duduković, C.S. Lo, Conversion of methane and carbon dioxide to higher value products, Ind. Eng. Chem. Res. 50 (12) (2011) 7089–7100.
[7] A. Erdöhelyi, et al., Catalytic reaction of methane with carbon dioxide over supported palladium, Appl. Catal. A Gen. 108 (2) (1994) 205–219.
[8] Y. Han, et al., A kinetic study of vinyl acetate synthesis over Pd-based catalysts: kinetics of vinyl acetate synthesis over Pd–Au/SiO and Pd/SiO catalysts, J. Catal. 232 (2) (2005) 467–475.
[9] E.M. Wilcox, G.W. Roberts, J.J. Spivey, Direct catalytic formation of acetic acid from CO_2 and methane, Catal. Today 88 (1–2) (2003) 83–90.
[10] D. Kumar, M.S. Chen, D.W. Goodman, Synthesis of vinyl acetate on Pd-based catalysts, Catal. Today 123 (1–4) (2007) 77–85.
[11] Y. Han, D. Kumar, D. Goodman, Particle size effects in vinyl acetate synthesis over Pd/SiO, J. Catal. 230 (2) (2005) 353–358.
[12] N. Macleod, J.M. Keel, R.M. Lambert, The effects of ageing a bimetallic catalyst under industrial conditions: a study of fresh and used Pd-Au-K/silica vinyl acetate synthesis catalysts, Appl. Catal. A Gen. 261 (1) (2004) 37–46.
[13] A. Vourros, et al., Carbon dioxide hydrogenation over supported Au nanoparticles: effect of the support, J. CO_2 Util. 19 (2017) 247–256.
[14] R. Sardar, et al., Gold nanoparticles: past, present, and future, Langmuir 25 (24) (2009) 13840–13851.
[15] M. Chen, et al., The promotional effect of gold in catalysis by palladium-gold, Science 310 (5746) (2005) 291–293.
[16] Y. Huang, et al., A comprehensive comparative DFT study on adsorption and reactions involved in vinyl acetate synthesis from acetoxylation of ethylene on pure Pd(100) and Pd-Au(100): elucidating the role of Au, Appl. Surf. Sci. 387 (2016) 1021–1028.
[17] D.-S. Lee, Y.-W. Chen, The mutual promotional effect of Au–Pd/CeO2 bimetallic catalysts on destruction of toluene, J. Taiwan Inst. Chem. Eng. 44 (1) (2013) 40–44.
[18] M. Chen, et al., The nature of the active site for vinyl acetate synthesis over Pd–Au, Catal. Today 117 (1–3) (2006) 37–45.
[19] B. Gleich, M.R., R.J.. Behm, Correlation between local substrate structure and local chemical properties: CO adsorption on well-defined bimetallic Au/Pd(111) ⦸surfaces, Surf. Sci., 1997. 38, 48–55.
[20] D.R. Mullins, The surface chemistry of cerium oxide, Surf. Sci. Rep. 70 (1) (2015) 42–85.
[21] K. Chang, et al., Application of Ceria in CO_2 conversion catalysis, ACS Catal. 10 (1) (2019) 613–631.
[22] K. Tomishige, M. Tamura, Y. Nakagawa, CO_2 conversion with alcohols and amines into carbonates, ureas, and carbamates over CeO2 catalyst in the presence and absence of 2-Cyanopyridine, Chem. Rec. 19 (7) (2019) 1354–1379.
[23] B. Ravel, M. Newville, Athena, Artemis, Hephaestus: data analysis for X-ray absorption spectroscopy using IFEFFIT, J. Synchrotron Radiat. 12 (4) (2005) 537–541.
[24] Newville, M., Larch: an analysis package for XAFS and related spectroscopies, J. Phys. Conf. Ser., 2013. 430, 012007.
[25] C. Binet, M. Daturi, Methanol as an IR probe to study the reduction process in ceria–zirconia mixed compounds, Catal. Today 70 (1) (2001) 155–167.
[26] K. Deng, et al., Studies of CO_2 hydrogenation over cobalt/ceria catalysts with in situ characterization: the effect of cobalt loading and metal–support interactions on the catalytic activity, Catal. Sci. Technol. 10 (19) (2020) 6468–6482.
[27] J.-b Wu, et al., Selective oxidation of methanol to methyl formate over bimetallic Au-Pd nanoparticles supported on SiO2, J. Fuel Chem. Technol. 47 (7) (2019) 780–790.
[28] S. Kawi, Y. Kathiraser, CO_2 as an oxidant for high-temperature reactions, Front. Energy Res. (2015) **3**.
[29] M.P. Casaletto, et al., XPS study of supported gold catalysts: the role of Au0 and Au +δ species as active sites, Surf. Interface Anal. 38 (4) (2006) 215–218.
[30] Z. Yin, et al., Supported bimetallic PdAu nanoparticles with superior electrocatalytic activity towards methanol oxidation, J. Mater. Chem. A 1 (2013) 32.
[31] Z. Li, et al., Formation and characterization of Au/Pd surface alloys on Pd(111), Surf. Sci. 601 (8) (2007) 1898–1908.
[32] S. Marx, A. Baiker, Beneficial interaction of gold and palladium in bimetallic catalysts for the selective oxidation of benzyl alcohol, J. Phys. Chem. C 113 (15) (2009) 6191–6201.
[33] L. Hilaire, et al., Interaction of oxygen and hydrogen with Pd-Au alloys: an AES and XPS study, Surf. Sci. 103 (1) (1981) 125–140.
[34] H. Duggal, et al., XANES spectroscopic studies at L3 edge of 79Au in its various chemical forms, Vacuum (2020) **176**.
[35] E.M. Slavinskaya, et al., Low-temperature CO oxidation by Pd/CeO2 catalysts synthesized using the coprecipitation method, Appl. Catal. B Environ. 166–167 (2015) 91–103.
[36] K.-i Shimizu, et al., The average Pd oxidation state in Pd/SiO2 quantified by L3-edge XANES analysis and its effects on catalytic activity for CO oxidation, Catal. Sci. Technol. 2 (2012) 4.
[37] I. Davoli, et al., The local electronic structure of PdO crystal and PdO catalyst supported on SiO2 and γ-Al2O3 from L3 and L1 x-ray absorption Pd edge in XANES spectra, Solid State Commun. 48 (5) (1983) 475–478.
[38] S. Colussi, P. Fornasiero, A. Trovarelli, Structure-activity relationship in Pd/CeO2 methane oxidation catalysts, Chin. J. Catal. 41 (6) (2020) 938–950.
[39] W. Lin, et al., Total oxidation of methane at low temperature over Pd/TiO2/Al2O3: effects of the support and residual chlorine ions, Appl. Catal. B Environ. 50 (1) (2004) 59–66.
[40] S. Okada, et al., Methane dissociative adsorption in catalytic steam reforming of methane over Pd/CeO2 in an electric field, Catal. Today 307 (2018) 272–276.
[41] F. Solymosi, et al., Decomposition of CH4 over supported Pd catalysts, J. Catal. 147 (1) (1994) 272–278.
[42] S.C. Su, J.N. Carstens, A.T. Bell, A study of the dynamics of Pd oxidation and PdO reduction by H2 and CH4, J. Catal. 176 (1) (1998) 125–135.
[43] A. Tompos, et al., Characterization of trimetallic Pt-Pd-Au/CeO2 catalysts combinatorial designed for methane total oxidation, Comb. Chem. High. Throughput Screen. 10 (1) (2007) 71–82.
[44] S. Nakamura, T. Yasui, The mechanism of the palladium-catalyzed synthesis of vinyl acetate from ethylene in a heterogeneous gas reaction, J. Catal. 17 (3) (1970) 366–374.
[45] J.M. Heitzinger, S.C. Gebhard, B.E. Koel, Chemisorption of ethylene and acetylene on ultrathin palladium films on molybdenum (100), J. Phys. Chem. 97 (20) (1993) 5327–5332.
[46] Y. Huang, et al., The influence of surface oxygen and hydroxyl groups on the dehydrogenation of ethylene, acetic acid and hydrogenated vinyl acetate on pure Pd(1 0 0): A DFT study, Appl. Surf. Sci. 388 (2016) 455–460.
[47] N.W. Cant, W.K. Hall, Catalytic oxidation: II. Silica supported noble metals for the oxidation of ethylene and propylene, J. Catal. 16 (2) (1970) 220–231.
[48] H. Gerberich, W.K. HALL, Oxidation of ethylene over palladium and palladium–gold alloys, Nature 213 (5081) (1967), 1120-1120.
[49] H. Gerberich, N.W. Cant, W.K. Hall, Catalytic oxidation: I. The oxidation of ethylene over Pd and Pd Au alloys, J. Catal. 16 (2) (1970) 204–219.
[50] H. Idriss, et al., Reactions of acetaldehyde on CeO2 and CeO2-supported catalysts, J. Catal. 155 (2) (1995) 219–237.
[51] M. Usman, W.M.A. Wan Daud, H.F. Abbas, Dry reforming of methane: influence of process parameters—a review, Renew. Sustain. Energy Rev. 45 (2015) 710–744.
[52] Z. Liang, et al., Low-temperature activation of methane on the IrO2(110), Surf. Sci. 356 (6335) (2017) 299–303.
[53] L. Yao, et al., Low-temperature CO_2 reforming of methane on Zr-promoted Ni/SiO2 catalyst, Fuel Process. Technol. 144 (2016) 1–7.
[54] L.-h Xiao, et al., Low-temperature catalytic combustion of methane over Pd/CeO2 prepared by deposition–precipitation method, Catal. Commun. 6 (12) (2005) 796–801.